CHEMISTRY OF MATERIALS
Article

Chem. Mater. **2010,** *22,* 3183–3191 3183
DOI:10.1021/cm100289d

Synthesis of Magnetite Nanooctahedra and Their Magnetic Field-Induced Two-/Three-Dimensional Superstructure

Ling Li,[†] Yang Yang, Jun Ding,* and Junmin Xue*

Department of Materials Science and Engineering, National University of Singapore, Singapore 117576, Republic of Singapore. [†]Current Address: Department of Materials Science and Engineering, Massachusetts Institute of Technology, Cambridge, MA 02139.

Received January 28, 2010. Revised Manuscript Received April 2, 2010

In this work, we report a robust wet-chemical route to synthesize monosized octahedron-shaped magnetite (Fe_3O_4) nanoparticles with average sizes ranging from 8 to ~430 nm. In other words, we are able to adjust the magnetic properties of the as-synthesized nanoparticles from superparamagnetic to single-domain to multidomain ferrimagnetic regimes. We also demonstrate a simple solvent-evaporation assembly process to obtain either 2D monolayer or 3D microrod superstructures made of 21 nm-sized nanooctahedra by applying a weak magnetic field (~0.06 T) in the horizontal or vertical direction, respectively. The as-obtained 2D monolayer assembly not only exhibits a long-range translational order (hexagonal close packing) but also has a high degree of crystallographic orientational order (⟨111⟩ texture normal to the substrate). Large-area assemblies (up to $10 \times 10\ \mu$m) can be formed on various substrates, for example, silicon substrates and carbon films of transmission electron microscopy copper grids, as demonstrated. By changing the magnetic field to the vertical direction, uniform 3D microrod superstructures with an aspect ratio of approximately 5 are obtained, and they also exhibit the specific crystallographic orientations.

I. Introduction

One of the challenges for modern chemists and materials scientists is to control and manipulate the shapes of materials on the nanometer scale, as different shapes of the nanostructures can introduce novel electronic, optical, or magnetic properties, compared with their spherical counterparts.[1−4] Substantial progress has been made on the shape-controlled synthesis of semiconductor nanocrystals, and typical nonspherical examples include triangles, rods, cubes, arrows, and tetrapods.[5−8] Moreover, nonspherical metallic Au or Ag nanoparticles have been found to shift their surface plasmon frequency drastically, making them useful for multicolor diagnosis and other optical devices.[9−12] Magnetic iron oxide nanoparticles (e.g., magnetite and maghemite) comprise another important class of nanostructured materials, which have widespread applications as diverse as environmental remediation, magnetic recording and bimolecular tagging, imaging, and sensing.[13−16] Compared to semiconductor and metallic nanocrystals, magnetic nanoparticles with nonspherical shapes demonstrate more appealing anisotropic magnetic properties.[17] Apart from the most common spherical shape, magnetic iron oxide nanoparticles with cubic, tetra-pod, tubular, triangular, ring/tube-like, octahedral, and pyramidal shapes have been reported.[18−21]

Despite the efforts described above to enrich the library of the shapes of iron oxide nanostructures, the size range of the products obtained through any single route is usually limited. To the best of our knowledge, there has been no direct synthesis of nonspherical iron oxide particles with

*To whom all correspondence should be addressed. E-mail: msedingj@nus.edu.sg; msexuejm@nus.edu.sg.

(1) Wang, Z. L. *Adv. Mater.* **1998**, *10*, 13–30.
(2) Jana, N. R.; Gearheart, L.; Murphy, C. J. *J. Phys. Chem. B* **2001**, *105*, 4065–4067.
(3) Tao, A. R.; Habas, S.; Yang, P. D. *Small* **2008**, *4*, 310–325.
(4) Jun, Y. W.; Choi, J. S.; Cheon, J. *Angew. Chem., Int. Ed.* **2006**, *45*, 3414–3439.
(5) Peng, X. G.; Manna, L.; Yang, W. D.; Wickham, J.; Scher, E.; Kadavanich, A.; Alivisatos, A. P. *Nature* **2000**, *404*, 59–61.
(6) Manna, L.; Scher, E. C.; Alivisatos, A. P. *J. Am. Chem. Soc.* **2000**, *122*, 12700–12706.
(7) Li, L. S.; Hu, J. T.; Yang, W. D.; Alivisatos, A. P. *Nano Lett.* **2001**, *1*, 349–351.
(8) Jun, Y. W.; Lee, S. M.; Kang, N. J.; Cheon, J. *J. Am. Chem. Soc.* **2001**, *123*, 5150–5151.
(9) Gao, J. X.; Bender, C. M.; Murphy, C. J. *Langmuir* **2003**, *19*, 9065–9070.
(10) Liao, H. W.; Hafner, J. H. *Chem. Mater.* **2005**, *17*, 4636–4641.
(11) Jin, R. C.; Cao, Y. W.; Mirkin, C. A.; Kelly, K. L.; Schatz, G. C.; Zheng, J. G. *Science* **2001**, *294*, 1901–1903.
(12) Jin, R. C.; Cao, Y. C.; Hao, E. C.; Metraux, G. S.; Schatz, G. C.; Mirkin, C. A. *Nature* **2003**, *425*, 487–490.
(13) Jeong, U.; Teng, X. W.; Wang, Y.; Yang, H.; Xia, Y. N. *Adv. Mater.* **2007**, *19*, 33–60.
(14) Xu, C. J.; Sun, S. H. *Polym. Int.* **2007**, *56*, 821–826.
(15) Gupta, A. K.; Gupta, M. *Biomaterials* **2005**, *26*, 3995–4021.
(16) Lu, A. H.; Salabas, E. L.; Schuth, F. *Angew. Chem., Int. Ed.* **2007**, *46*, 1222–1244.
(17) Chen, M.; Kim, J.; Liu, J. P.; Fan, H. Y.; Sun, S. H. *J. Am. Chem. Soc.* **2006**, *128*, 7132–7133.
(18) Cheon, J. W.; Kang, N. J.; Lee, S. M.; Lee, J. H.; Yoon, J. H.; Oh, S. J. *J. Am. Chem. Soc.* **2004**, *126*, 1950–1951.
(19) Shavel, A.; Rodriguez-Gonzalez, B.; Pacifico, J.; Spasova, M.; Farle, M.; Liz-Marzan, L. M. *Chem. Mater.* **2009**, *21*, 1326–1332.
(20) Jia, C. J.; Sun, L. D.; Luo, F.; Han, X. D.; Heyderman, L. J.; Yan, Z. G.; Yan, C. H.; Zheng, K.; Zhang, Z.; Takano, M.; Hayashi, N.; Eltschka, M.; Klaui, M.; Rudiger, U.; Kasama, T.; Cervera-Gontard, L.; Dunin-Borkowski, R. E.; Tzvetkov, G.; Raabe, J. *J. Am. Chem. Soc.* **2008**, *130*, 16968–16977.
(21) Kim, D.; Lee, N.; Park, M.; Kim, B. H.; An, K.; Hyeon, T. *J. Am. Chem. Soc.* **2009**, *131*, 454–455.

Published on Web 04/19/2010

sizes ranging from sub-10-nm up to several hundred nanometers. It is known that the superparamagnetic limit for magnetite is ~20 nm.[22,23] Most organic-phase synthesis methods reported previously have mainly focused on the size control of 4 to 20 nm from the thermal decomposition processes of iron acetylacetonate or iron oleate.[24] The synthesis of ferrimagnetic magnetite nanocubes from 22 to 160 nm has only recently been demonstrated.[21]

In addition to the rational synthesis of nanoparticles with desired morphologies and properties, the controlled nanoparticle assembly is another crucial step in designing functional nanodevices.[25−27] In particular, the assembly of magnetic nanoparticles has become an active research area due to its potential applications such as magnetic recording and biosensing.[25,28] It has been demonstrated that the crystallographic symmetry of the observed superlattices is strongly influenced by the shape of the nanoparticles.[29,30] As for the magnetic nanoparticles, their magnetic axis is closely related to their crystal structure. Therefore, the specific crystallographic orientation in an assembly influenced by the shapes of nanoparticles can finally lead to an aligned magnetic easy axis in the superstructures.[31] For example, Chen et al. demonstrated a self-assembly superlattice of FePt nanocubes with controlled texture and magnetic alignment.[17] Shape-dependent superlattice patterns, of either (100) or (110) texture, were obtained by using $MnFe_2O_4$ nanoparticles with cube- or polyhedron-like shapes, respectively.[31]

Here we report a facile synthesis of single crystalline octahedron-shaped magnetite (Fe_3O_4) nanoparticles bound with {111} planes through a thermal decomposition route. The particle size can be readily tuned from 8 to ~430 nm with narrow size distributions ($\sigma < 10\%$) without any seed-mediated growth or size sorting processes. Comprehensive experimental studies strongly suggest that the ratio between surfactant and precursor and the concentration of surfactant are the two key parameters for controlling the final morphology of nanoparticles. Kinetic studies using in situ magnetic moment measurement show a two-step increase in magnetic moment for the reaction solution, which is believed to be related to the fact that we obtain such monosized magnetite nanooctahedra. Magnetic property analysis indicates that r_0 and r_c are approximately 20 and 120 nm, respectively. More importantly, we demonstrate a simple solvent-evaporation assembly process to assemble the as-synthesized nanooctahedra in either 2D monolayer or 3D microrod superstructures with the assistance of an external magnetic field. Both the size and the shape of the nanoparticles and the direction of the magnetic field have profound effects on the final assembly patterns.

II. Experiment Procedure

Synthesis of Magnetite Nanooctahedra. In a typical synthesis of 53 nm-sized magnetite octahedral, iron(III) acetylacetonate (16 mmol, Fluka) and oleic acid (40 mmol, Fluka) were added to benzyl ether (50 mL, Sigma-Aldrich). The mixture was purged with nitrogen gas for 30 min to remove air at room temperature. The solution was then slowly heated to 165 °C for 30 min and finally heated to 280 °C to reflux the mixture for another 30 min. The mixture was cooled down to room temperature after reaction. For isolation of nanoparticles with size smaller than 20 nm, a standard solvent/nonsolvent (hexane/ethanol) approach was applied, while for particles larger than 20 nm, the particles could be readily separated directly through centrifugation after adding toluene due to aggregation that resulted from their ferrimagnetic property at room temperature.

Magnetic-Field Induced Assembly of 21 nm Magnetite Nanooctahedra. A droplet of the nanoparticle solution in the organic phase was carefully deposited onto the water surface in a Petri dish. The Petri dish was placed in a magnetic field generated by permanent magnets. The organic solvent was allowed to evaporate slowly at room temperature for two days. The as-formed 2D-/3D-superstructures were then transferred to solid substrates, for example, TEM copper grid with carbon film and silicon substrates, by lowering the water level with a syringe. The sample was subsequently vacuum-dried before TEM and SEM observations.

Characterizations. The morphology of the as-synthesized product was examined by using field-emission scanning electron microscopy (SEM; XL 30 FEG Philips, Hillsboro, OR). Transmission electron microscopy (TEM, JEOL-2010 at 200 kV) was employed to determine the morphology, size, and size distribution of the magnetite nanooctahedra. Magnetic properties were recorded by using a vibrating sample magnetometer (VSM) at room temperature. Particle phases were characterized using an X-ray diffractometer (XRD, D8 Advanced Diffractometer System, Bruker, Karlsruhe, Germany) with Cu Kα radiation.

III. Results and Discussion

Figure 1A presents a typical transmission electron microscopy (TEM) image of the as-synthesized magnetite nanooctahedra with an average size of 53 nm and standard deviation of 5.8%. The length between two opposite vertices was taken as the particle size, as shown in the schematic representation of an octahedron-shaped particle (Figure 1B). Particles with parallelogram projection shapes were taken for the particle size measurement to ensure reliable statistics, as shown in Figure S1 (Supporting Information). Figure 1C−E presents particles with different projection shapes dried on a copper grid, namely, hexagon, rectangle, and parallelogram, respectively. Schematic drawings of the corresponding projections of a perfect octahedron are also included, which closely resemble the TEM observations. The corresponding

(22) Kovalenko, M. V.; Bodnarchuk, M. I.; Lechner, R. T.; Hesser, G.; Schaffler, F.; Heiss, W. *J. Am. Chem. Soc.* **2007**, *129*, 6352–6353.
(23) Redl, F. X.; Black, C. T.; Papaefthymiou, G. C.; Sandstrom, R. L.; Yin, M.; Zeng, H.; Murray, C. B.; O'Brien, S. P. *J. Am. Chem. Soc.* **2004**, *126*, 14583–14599.
(24) Park, J.; An, K. J.; Hwang, Y. S.; Park, J. G.; Noh, H. J.; Kim, J. Y.; Park, J. H.; Hwang, N. M.; Hyeon, T. *Nat. Mater.* **2004**, *3*, 891–895.
(25) Sun, S. H.; Anders, S.; Thomson, T.; Baglin, J. E. E.; Toney, M. F.; Hamann, H. F.; Murray, C. B.; Terris, B. D. *J. Phys. Chem. B* **2003**, *107*, 5419–5425.
(26) Zeng, H.; Li, J.; Liu, J. P.; Wang, Z. L.; Sun, S. H. *Nature* **2002**, *420*, 395–398.
(27) Black, C. T.; Murray, C. B.; Sandstrom, R. L.; Sun, S. H. *Science* **2000**, *290*, 1131–1134.
(28) Sun, S. H.; Murray, C. B.; Weller, D.; Folks, L.; Moser, A. *Science* **2000**, *287*, 1989–1992.
(29) Jana, N. R. *Angew. Chem., Int. Ed.* **2004**, *43*, 1536–1540.
(30) Wang, Z. L.; Dai, Z. R.; Sun, S. H. *Adv. Mater.* **2000**, *12*, 1944–1946.
(31) Zeng, H.; Rice, P. M.; Wang, S. X.; Sun, S. H. *J. Am. Chem. Soc.* **2004**, *126*, 11458–11459.

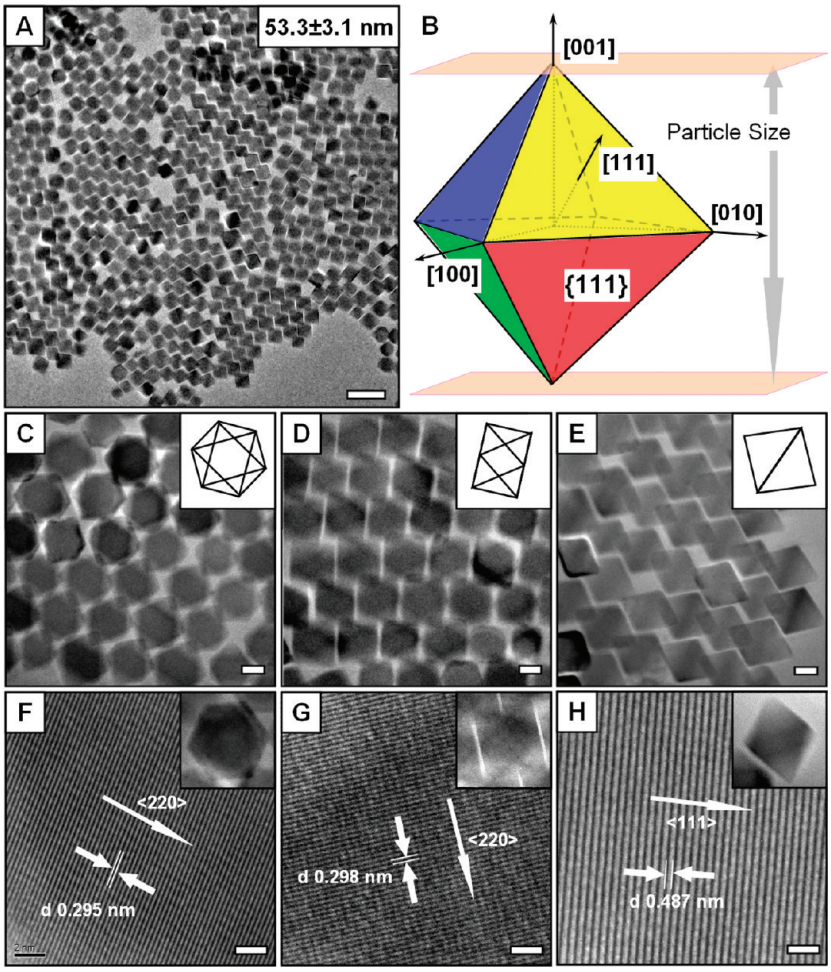

Figure 1. (A) Typical TEM image of 53 nm Fe_3O_4 nanooctahedra. (B) Schematic 3D model of one octahedron-shaped nanoparticle. TEM and HRTEM images of 53 nm Fe_3O_4 nanooctahedra with different projection shapes: (C, F) hexagonal (zone axis: ⟨111⟩), (D, G) rectangle (zone axis: ⟨112⟩), and (E, H) parallelogram (zone axis: ⟨110⟩). Scale bars: (A) 100 nm; (C−E) 20 nm; and (F−H) 2 nm.

high-resolution TEM (HRTEM) images are shown in Figure 1F−H. The lattice spacings in Figure 1F,G are measured at 0.295 and 0.298 nm, which are close to the standard *d* spacing of {220} at 0.297 nm for the cubic spinel-structured magnetite. The lattice spacing in Figure 1G is measured at 0.487 nm, which is close to the *d* spacing of {111} at 0.485 nm. Occasionally, five octahedra assembled together to form "star"-shaped structures by contacting their adjacent outer faces, and the HRTEM image further reveals that these outer faces are parallel to the {111} planes (Figure S2, Supporting Information). In addition, the projection angles are measured to be 70.5°, close to the theoretical value of the angle between two adjacent {111} planes. The sharp vertices suggest the formation of the perfect octahedron-shaped nanoparticles, in contrast to the Fe_3O_4 nanoparticles with truncated-octahedron shapes reported recently.[32,33] On the basis of the morphology characterizations described above, it is concluded that the as-obtained nanoparticles are single crystalline magnetite nanooctahedra, with their eight faces enclosed by {111} planes, as shown in Figure 1B.

The average particle size of the magnetite octahedra can be readily tuned from several hundred to sub-10 nm simply by adjusting the amount of iron precursor while keeping other parameters unchanged (Figure 2). For example, ~430 nm particles were obtained when 24 mmol of Fe(acac)$_3$ was used, as shown in a typical scanning electron microscopy (SEM) image (Figure 2**A**). The inset image presents a single perfect octahedron-shaped particle with one of its {111} planes facing upward. As the amount of precursor was gradually reduced from 20 to 8 mmol, magnetite octahedra with average particle sizes of 114, 21, 18, 8, and 6 nm were obtained. The as-synthesized particles have remarkably narrow size distributions, as indicated in the size histograms (Figure S3, Supporting Information). HRTEM images reveal that the nanoparticles with different sizes are all single crystalline (Figure S4, Supporting Information). It should be noted here that the octahedron geometry of the nanoparticles is gradually lost as the particle size decreases to less than 10 nm, and the 6 nm-sized nanoparticles are almost perfectly spherical in shape. The crystallographic information of the as-synthesized nanooctahedra with different sizes was studied using X-ray diffraction (XRD), as summarized in Figure 3. The positions and relative intensities of all diffraction peaks match

(32) Zheng, R. K.; Gu, H. W.; Xu, B.; Fung, K. K.; Zhang, X. X.; Ringer, S. P. *Adv. Mater.* **2006**, *18*, 2418–2421.
(33) Zhang, L. H.; Wu, J. J.; Liao, H. B.; Hou, Y. L.; Gao, S. *Chem. Commun.* **2009**, 4378–4380.

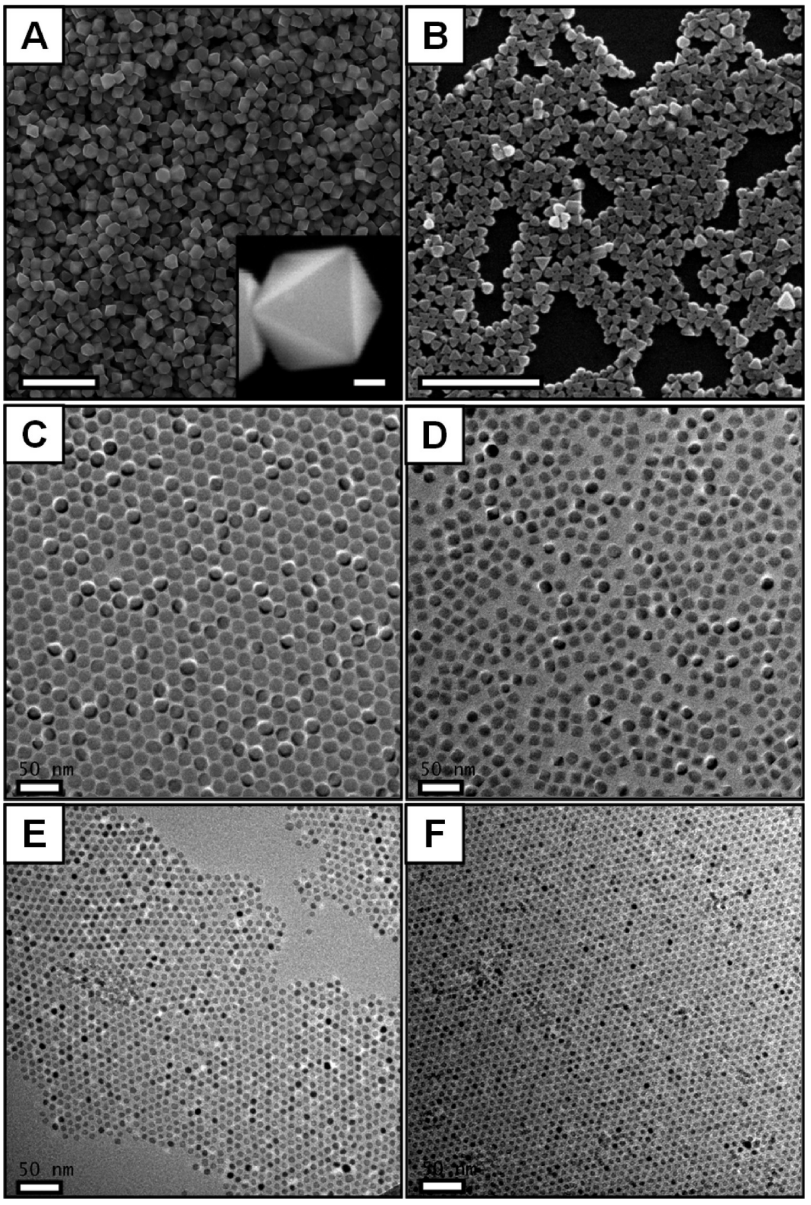

Figure 2. SEM (A, B) and TEM (C−E) images of the as-synthesized Fe_3O_4 nanooctahedra with different average sizes by adjusting the concentration of precursor ($Fe(acac)_3$): (A) ~430 nm (inset: SEM image of one single octahedron-shaped particle); (B) 114 nm; (C) 21 nm; (D) 18 nm; and (E) 8 nm. (F) TEM image of 6 nm-sized spherical nanoparticles. Scale bars: (A) 2 μm (inset: 100 nm); (B) 1 μm; and (C−F) 50 nm.

well with the standard magnetite diffraction data (JCPDS no. 19-0629). The crystalline sizes calculated from the (311) peak based on Scherrer's formula are comparable with the average sizes determined from TEM images, which further confirms that the as-synthesized nanoparticles are indeed single crystalline.

Magnetism is highly volume dependent because this property arises from the collective interaction of atomic magnetic dipoles.[34,35] The magnetic properties of the as-synthesized magnetite nanooctahedra with different sizes were studied using a vibrating sample magnetometer (VSM) (Figure 4). The size-dependent saturation magnetizations (m_s) were measured to be 95.20, 93.36, 86.84, 81.42, 73.51, 48.94, and 42.24 emu/g for 430, 114, 53, 21, 18, 8, and 6 nm-sized particles, respectively. The saturation magnetization of 430 nm-sized Fe_3O_4 particles is comparable with the bulk Fe_3O_4 (85−100 emu/g).[36,37] Additionally, compared with bulk magnetic materials, m_s for the particles with finite dimensions are considerably smaller due to the surface spin canting.[38,39] More specifically, the saturation magnetization of nanoparticles can be described as $m_s = M_s[(r - d)/r]^3$, where r is the particle size, M_s is the saturation magnetization of the corresponding bulk material, and d is the thickness of

(34) O'Handley, R. C. *Modern magnetic materials: principles and applications*; Wiley: New York, 2000.
(35) Spaldin, N. A. *Magnetic materials: fundamentals and device applications*; Cambridge University Press: Cambridge, U.K., 2003.
(36) Xuan, S. H.; Hao, L. Y.; Jiang, W. Q.; Song, L.; Hu, Y.; Chen, Z. Y.; Fei, L. F.; Li, T. W. *Cryst. Growth Des.* **2007**, *7*, 430–434.
(37) Zhang, J. H.; Kong, Q. H.; Du, J.; Ma, D. K.; Xi, G. C.; Qian, Y. T. *J. Cryst. Growth* **2007**, *308*, 159–165.
(38) Morales, M. P.; Veintemillas-Verdaguer, S.; Montero, M. I.; Serna, C. J.; Roig, A.; Casas, L.; Martinez, B.; Sandiumenge, F. *Chem. Mater.* **1999**, *11*, 3058–3064.
(39) Jiles, D. *Introduction to magnetism and magnetic materials*, 2nd ed.; Chapman and Hall: London, 1998;.

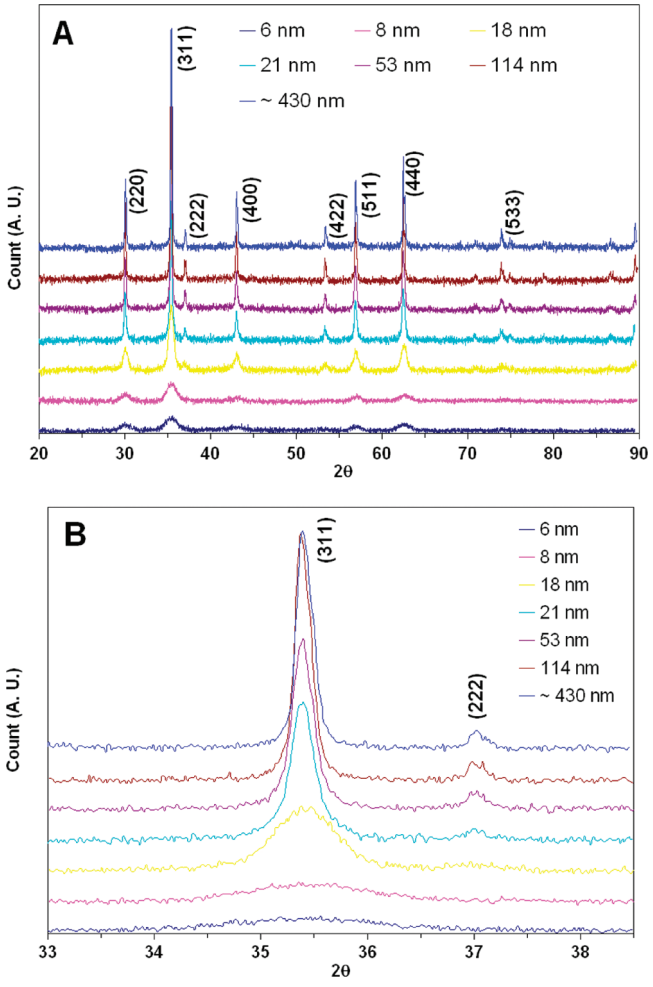

Figure 3. (A) X-ray diffraction (XRD) spectra of the as-synthesized magnetite nanooctahedra with different average sizes, and (B) the change of the (311) peak intensity of each class of nanoparticles. All samples were deposited on glass substrates from their hexane dispersions.

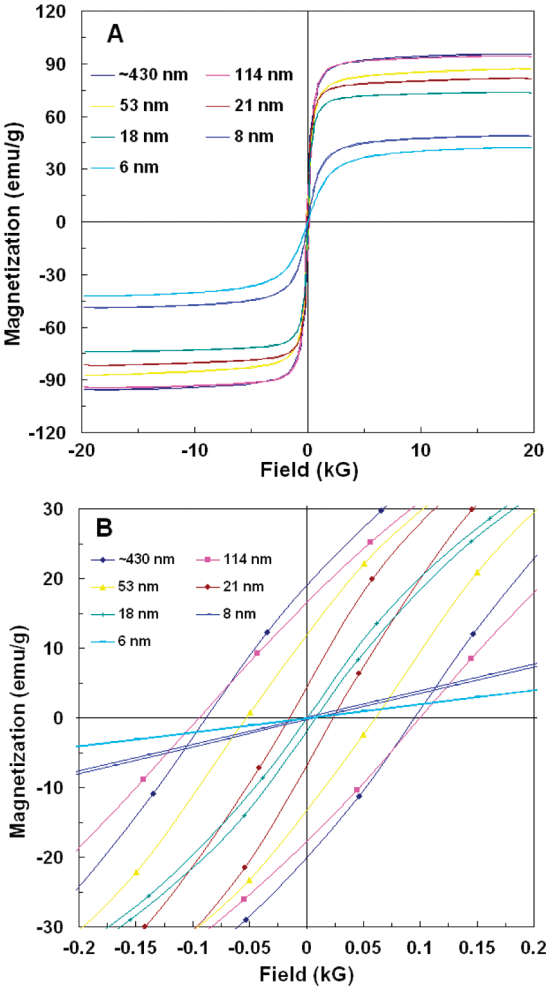

Figure 4. (A) Magnetization as a function of applied field for the powder samples of the as-synthesized magnetite nanooctahedra with different sizes at room temperature and (B) the magnetization-field curves at low applied field.

disordered surface layer. The linear correlation between $m_s^{1/3}$ and r^{-1} indicated by this equation is demonstrated in Figure S5 (Supporting Information). By fitting the curve, the values of M_s and d estimated to be 96.30 emu/g and 1.03 nm are close to other reported values.[34]

Three characteristic regimes have been observed for our magnetite particles due to their large size ranges, as shown in Figure S6 (Supporting Information). Magnetite nanoparticles with sizes of 6 and 8 nm are superparamagnetic at room temperature because of their zero coercivities. The very small but nonzero coercivity (4.25 Oe) observed for 18 nm-sized nanoparticles indicates that this size is close to the superparamagnetic limit size r_0, which is comparable with the previous reports.[21,22] The magnetites showed quasi-superparamagnetic behaviors with small coercivities when the particle sizes ranged from 18 to 25 nm. The coercivity then increases with size, reaches a maximum, and starts to decrease again. The decrease in coercivity is associated with the transition from single-domain to multidomain.[21,34] The single domain particle size is roughly estimated to be 120−150 nm according to the reported values for magnetites.[40] In addition, the transition of coherent rotation/curling may play an important role (as proposed for aspherical nanoparticles.[41] The difference in the magnetic properties of nanoparticles has dramatic effects on their colloidal stability: superparamagnetic nanoparticles form stable liquid dispersions at room temperature, while nanoparticles with sizes larger than 50 nm readily aggregate and settle at the bottom of solutions (Figure S7, Supporting Information). Our method offers a simple route to synthesize magnetite with different sizes that are either superparamagnetic or single- or multi-domain ferrimagnetic, depending on their sizes. The as-synthesized Fe_3O_4 nanoparticles can be used as an excellent model system for studying the size-dependent magnetic properties of magnetite because (1) they have a large average size range from sub-10 to several hundred nanometers and (2) within each size group, the size distribution is small.

We have also investigated the formation mechanism of the octahedron-shaped nanoparticles through the study

(40) Klabunde, K. J. *Nanoscale materials in chemistry*; Wiley-Interscience: New York, 2001; Chapter 11, p 292.

(41) Skomski, R.; Kashyap, A.; Sorge, K. D.; Sellmyer, D. J. *J. Appl. Phys.* **2004**, *95*, 7022.

of different reaction conditions. When the amount of iron precursor was increased beyond 40 mmol, nonmagnetic red-colored particles were obtained, although a small portion of black powder could be separated magnetically. XRD analysis indicates that the red colored particles are in hematite phase (JCPDS no. 33-0664), and SEM images reveal that the particles have undefined faceted structures (Figure S8, Supporting Information). The magnetically separated particles are cube-shaped magnetite particles with an average size of ~200 nm (Figure S9, Supporting Information). When the amount of iron precursor was reduced to less than 4 mmol, no particles but gel-like products with dark brown color were obtained. These findings indicate that to obtain the well-defined octahedron-shaped nanoparticles with a pure magnetite phase, the molar ratio between precursor and surfactant must be within a specific range, that is, 0.6−0.2. When the ratio is larger than 0.6, the amount of Fe^{2+} reduced from Fe^{3+} is not enough to form the stoichiometric magnetite phase. It has been suggested and partially proven experimentally that the trace amount of CO, H_2, and carbon produced by the thermal decomposition of the iron−oleate complex is responsible for the reduction of Fe^{3+} to Fe^{2+}.[42] We therefore speculate that oleic acid serves as both the reducing and capping agent in this synthesis,[43] and the precursor/surfactant ratio must be less than 0.6 for the purpose of enough reduction of Fe^{3+} to Fe^{2+}. Moreover, the concentration of surfactant in the reaction solution must be larger than 0.35 M. Irregular-shaped particles with decreasing sizes were obtained when the surfactant was continuously reduced from 0.35 to 0.07 M while keeping other parameters unchanged (Figure S10, Supporting Information). A similar trend has been found for the synthesis of cubic $MnFe_2O_4$, which has a similar structure as magnetite.[31] Hou et al. have also found that oleic acid facilitates the growth of ⟨100⟩ over the ⟨111⟩ direction, which leads to the formation of FeO truncated octahedron nanoparticles.[44] Here in our synthesis, the presence of excess oleic acid facilitates the final formation of faceted octahedron-shaped structures.

The reaction kinetics was studied by monitoring the change in the magnetic moment of the reaction solution during the synthesis process. As shown in Figure S11 (Supporting Information), the magnetic moment remained relatively unchanged for 5 min at 280 °C before a small increase was observed. Another sharp increase in the magnetic moment was detected when the reaction was allowed for 35 min. A similar two-step increase in magnetic moment was also observed when iron oxide nanoparticles were formed during the heating-up process of the iron−oleate complex.[42] The two increases in magnetic moment correspond to two processes, the formation of intermediate monomers and the growth of nanoparticles.[42] The detailed growth mechanism is not completely understood at this stage. However, the above experimental observations strongly suggest the importance of the concentration of surfactant and the heating profile in the fabrication of shape-controlled particles with narrow size distributions.

As a result of their uniform sizes, the as-synthesized Fe_3O_4 nanooctahedra can be used as excellent building blocks to obtain nanoparticle superlattices. The two most-frequently applied methods, evaporation assembly[30,45] and Langmuir−Blodgett assembly,[46−49] usually result in close-packed isotropic assembly structures. Moreover, these techniques lack the controllability over the crystallographic orientation in the superlattices, although it has been demonstrated that the shapes of nanoparticles play a significant role in obtaining orientation-specific superstructures. We have also obtained the hexagonal close-packed 2D superlattice using nearly spherical 6 nm nanoparticles by slowly evaporating the solvent (Figure S12, Supporting Information). In this case, the directional magnetostatic interaction among the nanoparticles does not play a major role in the assembly process at room temperature due to superparamagnetism.[32] The complete diffraction rings for this assembly pattern also indicate that the as-formed 2D layer does not have any specific crystallographic orientation.

Unlike superparamagnetic nanoparticles, 53 nm Fe_3O_4 nanooctahedra aggregate together to form localized patterns due to the strong magnetic dipolar interactions. Several assembly patterns were observed: (1) single-layered patterns with different zone axes (Figure 1C−E); (2) chain-like structures formed by connecting opposite vertices of the nanooctahedra (Figure S13, Supporting Information); and (3) close-packed superlattices (Figure S14, Supporting Information). It is known that magnetotatic bacteria have aligned 1D structures similar to those of ferrite nanocrystals, which are used by the bacteria to align and swim along the earth's magnetic field.[50] As the nanoparticles are prone to strong dipolar interactions, the size of the assembly patterns described above is usually small, that is, less than 50 particles in the superstructures. The self-assemblies with strong magnetic interactions among the nanoparticles are severely affected by the local magnetic environment created by the neighboring nanoparticles. This directional interaction enables the magnetic nanoparticles to form one-dimensional chains/wires or closed-packed aggregates. Normal assembly strategies, for example, the slow evaporation of solvents, have minimum effects on producing large-scale assemblies. Therefore, it is difficult to obtain superstructures

(42) Kwon, S. G.; Piao, Y.; Park, J.; Angappane, S.; Jo, Y.; Hwang, N. M.; Park, J. G.; Hyeon, T. *J. Am. Chem. Soc.* **2007**, *129*, 12571–12584.
(43) Xu, Z. C.; Shen, C. M.; Hou, Y. L.; Gao, H. J.; Sun, S. H. *Chem. Mater.* **2009**, *21*, 1778–1780.
(44) Hou, Y. L.; Xu, Z. C.; Sun, S. H. *Angew. Chem., Int. Ed.* **2007**, *46*, 6329–6332.
(45) Lu, W. G.; Liu, Q. S.; Sun, Z. Y.; He, J. B.; Ezeolu, C. D.; Fang, J. Y. *J. Am. Chem. Soc.* **2008**, *130*, 6983–6991.
(46) Kim, F.; Kwan, S.; Akana, J.; Yang, P. D. *J. Am. Chem. Soc.* **2001**, *123*, 4360–4361.
(47) Whang, D.; Jin, S.; Wu, Y.; Lieber, C. M. *Nano Lett.* **2003**, *3*, 1255–1259.
(48) Gattas-Asfura, K. M.; Constantine, C. A.; Lynn, M. J.; Thimann, D. A.; Ji, X. J.; Leblanc, R. M. *J. Am. Chem. Soc.* **2005**, *127*, 14640–14646.
(49) Kwan, S.; Kim, F.; Akana, J.; Yang, P. D. *Chem. Commun.* **2001**, *5*, 447–448.
(50) Bazylinski, D. A.; Frankel, R. B. *Nat. Rev. Microbiol.* **2004**, *2*, 217–230.

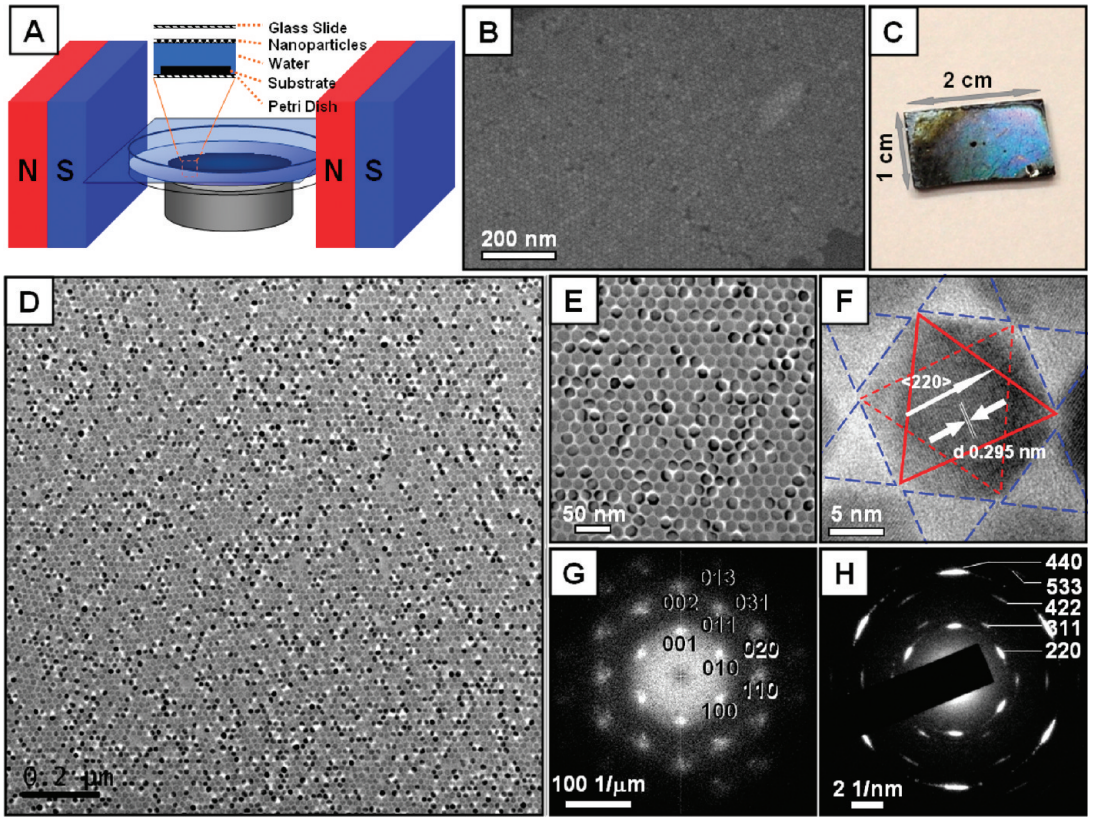

Figure 5. (A) Schematic illustration of the magnetic-field-induced assembly process. The toluene solution dispersed with 21 nm Fe_3O_4 nanooctahedra was carefully deposited on the water surface. After the solvent was evaporated off slowly in two days, the as-formed 2D monolayer was transferred onto solid substrates by lowering the water level carefully. (B) SEM image, (C) photograph, and (D−E) TEM images of the 2D monolayer assembly. (F) HRTEM TEM image of one single nanoparticle in the assembly (solid red triangle: (111) plane at the top; dashed red triangle: (111) plane at the bottom; solid blue triangles: interparticle spaces). Fast Fourier transformation (FFT) pattern (G) and selected area electron diffraction (SAED) pattern (H) of the 2D assembly corresponding to Figure 3E.

with a long-range order using ferrimagnetic nanoparticles at room temperature.

The above observation and analysis led us to study the assemblies of the quasi-superparamagnetic magnetites. In this work, 21 nm-sized magnetite nanooctahedra were selected. The larger saturation magnetization of 21 nm nanoparticles (81.42 emu/g) compared to 6 nm nanoparticles (42.24 emu/g) is usually favored for practical applications. In addition, the interparticle magnetic dipolar interaction is smaller than that of 53 nm nanoparticles due to the fact that 21 nm is closer to the superparamagnetic limit. We also expect that the octahedron shape of the nanoparticles may play an important part in determining the assembly patterns. As a result of the weak dipolar interactions, two-layered structures with a short-range order were observed when the nanoparticle dispersion was slowly dried on the TEM copper grids (Figure S15A, Supporting Information). This double-layered structure can reduce the dipolar interaction by having two opposite magnetic moments between the particles at the top and bottom, as shown in Figure S15B (Supporting Information). However, even though the evaporation process was allowed to be very slow, we were not able to obtain any superlattices with the long-range order. Therefore, these findings suggest that the interparticle magnetic interaction between 21 nm nanoparticles, which is smaller than that of 53 nm nanoparticles, still prevents large-area assemblies.

To form superlattices with the long-range order using 21 nm-sized nanoparticles, we need to either reduce the interparticle magnetic interaction or introduce another interaction that can effectively dominate the magnetic dipolar interaction during the assembly process. Therefore, we developed a simple assembly process with the help of an external magnetic field to obtain either 2D monolayer or 3D microrod superstructures. A schematic setup for preparing the 2D monolayer of magnetite nanooctahedra onto solid substrates is shown in Figure 5A. A horizontal magnetic field (~0.06 T), generated by permanent magnets, was applied parallel to the water level in a Petri dish. A dilute solution of 21 nm Fe_3O_4 nanoparticles dispersed in toluene was carefully deposited onto the water surface, and it was allowed to evaporate for two days. The water level was then gradually lowered using a syringe, and the as-formed nanoparticle monolayer was transferred onto the substrate at the bottom of the Petri dish. Figure 5B,C shows the SEM image and photograph of the as-prepared monolayer assembly made of 21 nm nanoparticles on silicon substrates. The TEM images in Figure 5D−F present the typical monolayer assembly deposited onto the copper grid, demonstrating a hexagonal close-packed structure. The size of the assembly can reach as large as 10 × 10 μm, corresponding to more than 4×10^5 nanooctahedra (Figure S16, Supporting Information). The corresponding fast Fourier transformation (FFT) image indicates a sixfold

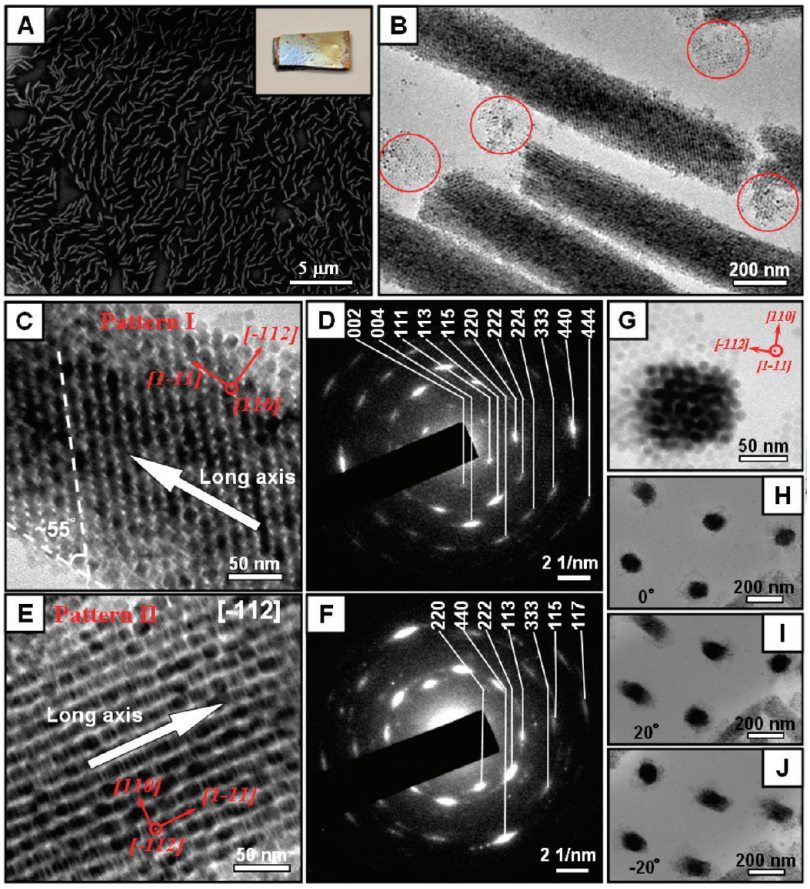

Figure 6. (A) SEM image of the 3D microrod superstructures on a silicon substrate (Inset: photograph of the as-prepared sample). (B) TEM image of the microrods (red circles: the bases of microrods). TEM images (C, E) and corresponding SAED patterns (D, F) demonstrating two distinct patterns viewed from two perpendicular directions (C, D: Pattern I, [110]; E, F: Pattern 2, [$\bar{1}$12]). (G) TEM image of a microrod from the top (the crystallographic directions are indicated). (H−J) TEM images showing the change in projection shapes of the vertical microrods when the sample was rotated at different angles: (H) 0°, (I) 20°, and (J) −20°.

symmetry, which agrees with the hexagonal packing pattern (Figure 5G).[30] Moreover, the equivalent lattice spacing measured from the FFT pattern is comparable with the actual particle size.

Hexagon projection shapes were observed for the majority of the nanoparticles in the 2D monolayer, indicating that a preferred ⟨111⟩ texture normal to the substrate was formed. The {220} plane system observed in the HRTEM image also suggests the zone axis was ⟨111⟩ (Figure 5F). The distinct texture of the magnetic field-induced 2D monolayer can also be interpreted by evaluating the corresponding SAED pattern (Figure 5H). The single-crystal-like diffraction spots for the superlattice can be indexed according to the ⟨111⟩ direction of magnetite, which is different from the ring-like patterns resulting from the randomly distributed nanoparticles. This difference indicates that the as-obtained 2D nanoparticle monolayer assemblies not only have the regular translational symmetry but also the same crystallographic orientation among the nanoparticles. The 2D monolayer made of superparamagnetic iron oxide nanocubes with a ⟨100⟩ texture has been obtained with/without using external magnetic field recently.[51,52] Finally, ridge-like multilayers of nanoparticle assemblies were observed when the magnetic field was not parallel with the water level (Figure S17, Supporting Information).

In addition to the 2D monolayer assembly, 3D microrod superstructures can be obtained by simply changing the magnetic field to the vertical direction. Figure 6A shows the SEM image for the as-obtained microrods uniformly distributed on a silicon substrate, in which the rod length, diameter, and aspect ratio are measured to be ~1.2 μm, ~250 nm, and 5, respectively. TEM observations (Figure 6B) indicate that all the nanoparticles were incorporated into the 3D superstructures during the assembly process, and the nanoparticle monolayer indicated by the red circles is believed to be the bases of the microrods, which can be visualized more clearly in the large-area TEM images (Figure S18, Supporting Information). Two distinct assembly patterns have been observed, and their corresponding SAED patterns are also presented (Pattern I: Figure 6C,D, Pattern II: Figure 6E, F). Single-crystal-like SAED patterns indicate that the nanoparticles in the microrod have strong crystallographic alignments similar to the 2D monolayer case, and the zone axes are determined to be ⟨110⟩ and ⟨112⟩, respectively. Superlattices similar to Pattern I have been observed for truncated-octahedron-shaped magnetite

(51) Ahniyaz, A.; Sakamoto, Y.; Bergstrom, L. *Proc. Natl. Acad. Sci. U. S.A.* **2007**, *104*, 17570–17574.
(52) Yang, H.; Hasegawa, D.; Takahashi, M.; Ogawa, T. *IEEE Transactions on Magn.* **2008**, *44*, 3895–3898.

nanoparticles.[32] A detailed 3D reconstruction of the assembly patterns indicates that the two patterns are from the same superstructure but viewed in two perpendicular directions, that is, [110] for Pattern I and [$\bar{1}$12] for Pattern II (Figure S19, Supporting Information). Figure 6**G** presents a vertical microrod under TEM that gives a clear top view of the superstructures. Two perpendicular directions are also indicated, from which the two assembly patterns can be observed. Figure 6H−J demonstrates that the projection geometry changes upon the rotation of the TEM sample holder. It has been shown that the attractive dipolar interaction between nanoparticles along the field direction and the repulsive interactions along the direction perpendicular to the field direction have facilitated the anisotropic growth of nanoparticle superlattices along the field direction, leading to the formation of rod-like superstructures.[53] In our case, the shape of nanoparticles also plays a significant role in determining the final assembly pattern and crystallographic orientation.

IV. Conclusions

In summary, we demonstrate a facile synthesis of single-crystalline magnetite nanocrystals with octahedron shapes enclosed by {111} planes via a one-step thermal decomposition route. The average particle sizes, from 8 to ~430 nm, can be finely controlled by modulating the precursor/surfactant ratio. This method offers a simple way to directly obtain monosized magnetite nanooctahedra that span both superparamagnetic and ferrimagnetic regimes. The surfactant/precursor ratio and the concentration of surfactant are the two crucial parameters for synthesizing the octahedron-shaped nanoparticles with uniform sizes. Further experimental and theoretical study is needed to fully understand the formation thermodynamics and kinetics. In addition, we demonstrate a simple procedure to obtain 2D monolayer and 3D microrod superlattices using 21 nm-sized nanooctahedra in the presence of a weak magnetic field (~0.06 T). The experimental findings strongly suggest that both the intrinsic properties of the nanoparticles (size and shape) and the direction of the external magnetic field have profound effects on the final assembly patterns. The strategy to use magnetite nanooctahedra to form stable superlattices may be extended to other magnetic systems, which may find potential applications such as high density data storage.

Supporting Information Available: Additional figures as mentioned in the text (PDF).

This material is available free of charge via the Internet at http://pubs.acs.org.

(53) Park, J. I.; Jun, Y. W.; Choi, J. S.; Cheon, J. *Chem. Commun.* **2007**, *47*, 5001–5003.